IEEE Access
Multidisciplinary ⋮ Rapid Review ⋮ Open Access Journal

Received 3 December 2025, accepted 22 December 2025, date of publication 29 December 2025, date of current version 2 January 2026.

Digital Object Identifier 10.1109/ACCESS.2025.3649166

RESEARCH ARTICLE

Full Band CP Ferrite-Based Satellite Feed Structure for LEO Satellite Applications

MAHMOUD GADELRAB[1], (Student Member, IEEE), SHOUKRY I. SHAMS[1], (Senior Member, IEEE), MAHMOUD ELSAADANY[2], (Senior Member, IEEE), AND GHYSLAIN GAGNON[2], (Senior Member, IEEE)

[1]Electrical and Computer Engineering Department, Concordia University, Montreal, QC H3G 1M8, Canada
[2]Département de Génie Électrique, École de technologie supérieure, Montreal, QC H3X 1K3, Canada

Corresponding author: Mahmoud Gadelrab (Mahmoud.gadelrab@ieee.org)

ABSTRACT Circular polarization (CP) systems are vital in modern satellite communication. They reduce multipath interference, maintain the purity of polarization, and ensure reliable signal transmission and reception across a wide range of frequencies. Low Earth Orbit (LEO) satellites are becoming popular in the wireless communications field. They will play a significant role in future wireless communication networks. At the center of these systems, orthomode transducers (OMTs) and polarizers are essential components. They efficiently separate and convert orthogonal modes into right-hand and left-hand circularly polarized signals. However, conventional OMT and polarizer designs often struggle to achieve a compact size, a wide bandwidth, and high isolation simultaneously. This paper combines a high-performance OMT with a ferrite-based polarizer optimized for the 19.5–29.5 GHz band. The proposed OMT demonstrates low insertion loss, high return loss, and a small footprint. These features tackle the limitations of traditional twofold designs. The ferrite polarizer, made of segmented slabs and matching posts, provides a flat phase response and excellent thermal stability. Experimental measurements of the built OMT closely match the simulations. When paired with the ferrite polarizer, the overall CP system shows improved bandwidth, axial ratio, and isolation, making it a strong candidate for future satellite communication systems.

INDEX TERMS Circular polarization, ferrite-loaded waveguide, LEO feeding structure, system evaluation, two-fold OMT, waveguide polarizer.

I. INTRODUCTION

Nowadays, with the growing need for information, and the importance of the transceiver in telecommunications, a lot of research is being done on antenna design as a key part of a transceiver system [1], [2], [3]. Satellite transceivers are important for many applications because they offer global coverage and support mobility. Large companies are competing for a share of the satellite internet market, which is likely to be a major player in future internet services. These companies plan to launch many small satellites to orbit the Earth in what is known as Low-Earth Orbit (LEO) [4], [5]. Satellite feeds are essential for the effective and reliable operation of satellite communication systems. The design and effectiveness of the feeding structure significantly influence the overall quality of communication links, data rates, and signal reception sensitivity. An optimally designed feeding structure reduces signal losses and lowers interference, thus enhancing the overall communication performance [6], [7]. As satellite communication systems advance and require higher data rates, the importance of optimized feeding structures becomes increasingly paramount. Moreover, innovations in feeding structure technology support multiband and multi-polarized systems, allowing satellites to accommodate a variety of applications and fulfill the requirements of contemporary communication networks [8].

The satellite feed structure is responsible for transmitting and receiving signals across wide frequency ranges while preserving polarization purity and minimizing insertion loss. Circular polarization (CP) is particularly beneficial for Low

The associate editor coordinating the review of this manuscript and approving it for publication was Tutku Karacolak.

Earth Orbit (LEO) satellite systems, as it reduces multipath effects in wireless channels compared to linear polarization of similar radiation characteristics [9], [10], [11]. A central component of any dual-polarized CP feed is the orthomode transducer (OMT), which separates/combines two orthogonal linear modes with high isolation. Conventional OMTs—whether based on Bøifot junctions, turnstile junctions, or other waveguide topologies—have demonstrated excellent electrical performance and isolation levels approaching 50 dB [12]. However, these achievements often come at the cost of large cross-sectional dimensions, intricate internal junctions, and complex power-combiner networks, all of which increase fabrication difficulty and mass [13], [14], [15], [16], [17].

One conventional solution is to cascade the OMT with a 90-degree polarizer, which converts the orthogonal linear modes into right-hand and left-hand circularly polarized (RHCP and LHCP) waves. Recent research shows rapid progress in waveguide polarizer designs for circularly polarized antenna systems [18]. The waveguide polarizer is a two-port device that produces the required 90° phase shift between orthogonal modes by introducing carefully engineered discontinuities—such as irises, corrugations, ridges, or posts—within circular or square waveguides. These structures can provide broad bandwidth and good polarization purity, but typically require multiple internal features and relatively large physical dimensions. Variants that rely on more compact elements, for example, using only circular posts, reduce size but sacrifice operating bandwidth [19], [20]. Hybrid approaches that combine different discontinuities seek to balance these trade-offs, achieving improved matching and phase control while still facing limits in overall bandwidth and fabrication complexity [21], [22].

Waveguide phase shifters offer distinct advantages over other implementations owing to their high power-handling capability, compact form factor, and nearly flat phase response across the operational bandwidth. Among these, the rectangular waveguide loaded with horizontal ferrite slabs is one of the most widely adopted designs. Incorporating horizontal ferrite slabs enhances thermal dissipation and minimizes phase variation over frequency [23], [24], [25], [26]. Extending this concept to a square waveguide geometry enables the realization of ferrite-based polarizers. Such devices leverage the nonreciprocal properties of ferrite materials to achieve broadband 90° phase shifting while maintaining a low profile and excellent thermal stability. However, existing ferrite polarizers rarely satisfy the stringent 19.5–29.5 GHz full-band requirement in a single, space-qualified unit, highlighting a clear opportunity for innovation in both material engineering and device architecture.

This paper presents the design and validation of a novel compact circular polarization (CP) system that integrates an orthomode transducer (OMT) with a ferrite-based polarizer for satellite communication applications. The proposed OMT demonstrates low insertion loss, high return loss, and reduced size, overcoming the limitations of conventional twofold OMTs. The ferrite polarizer utilizes segmented slabs with matching posts, resulting in a flat phase response and improved thermal stability. A prototype of the OMT was fabricated and experimentally measured, showing strong agreement with simulated results. These measurements were then incorporated into CST simulations to evaluate the performance of the polarizer. Across the 19.5–29.5 GHz frequency band, the integrated CP system achieves a balanced performance in terms of bandwidth, matching level, axial ratio, and isolation.

II. CIRCULAR POLARIZED SYSTEMS

Circular polarization (CP) has become a key feature of most communication systems, including satellite telecommunications, television broadcasting, mobile networks, and wireless data networks. Three representative feed configurations for generating circularly polarized waves are reported in the literature [27] as shown in Figure 1. The first configuration is a Waveguide polarizer with an orthomode transducer (OMT). In this system, the waveguide polarizer first converts the circularly polarized signal into orthogonal linear components, which an OMT subsequently separates [28]. The second configuration includes an OMT with two diplexers and two 90° hybrid couplers. In this arrangement, the OMT is followed by diplexers that isolate the transmit and receive frequency bands. A set of 90° hybrid couplers then transforms the linearly polarized signals back to CP [29]. The last one is the Septum polarizer or circularly polarized OMT, which is considered the most compact alternative. It employs a CP capable of transmitting and receiving both RHCP and LHCP signals by inserting a septum in the common port.

The block diagrams in Fig. 1 show the different circular polarization (CP) feed architectures. In the first two setups, a two-fold OMT combines with either a polarizer or a hybrid coupler to create CP. These methods enable wide operational bandwidths and deliver strong performance, but they also result in larger structures. In the coupler-based setup, the operation is limited to sub-bands instead of the full OMT bandwidth because the couplers split the spectrum into two separate bands where CP occurs. To extend this method for three-band operation, three couplers would need to be integrated with a single OMT, which would add complexity and size. A better solution is to use a full-band polarizer, which covers the entire frequency range in a compact design. This reduces volume while still maintaining broadband CP performance [28], [30]. The third configuration offers a smaller and simpler feed for satellite applications. These septa provide a graded transition and achieve a good matching level; however, most of the proposed designs are limited in the operation bandwidth or have high axial ratio levels. Moreover, wideband implementations described in the literature typically require transition sections for seamless integration with the antenna [31], [32].

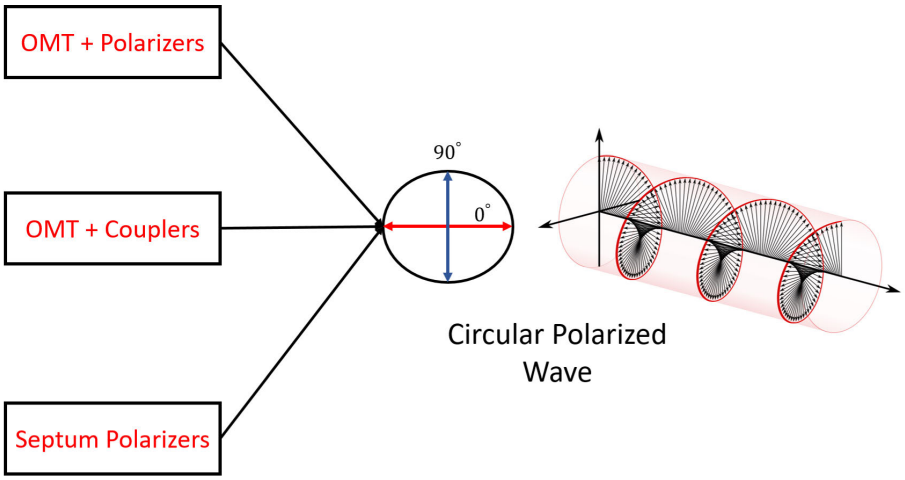

FIGURE 1. The most common satellite feeding systems producing circular polarized wave.

A. SYSTEM SPECIFICATIONS

In this article, the first configuration will be deployed, which integrates a two-fold OMT, a novel ferrite polarizer, and a corrugated horn antenna. The overall specification goal for this system is shown in Table 1, where the proposed frequency band covers the K and Ka bands 19.5-29.5 GHz. The intended frequency bands for LEO communication are located in these bands or in the QV bands [28]. The intended matching level on both ports is around 21 dB. The isolation between the left-handed and right-handed ports for both cases is around 40 dB. The other key design targets are an axial ratio (AR) below 1 dB or better. The overall insertion loss for this system should be approximately 0.7 dB, which contributes to the overall efficiency of the system.

TABLE 1. CP system specifications.

Frequency (GHz)	19.5-29.5
Return Loss (dB)	21
Insertion Loss (dB)	0.7
Axial Ratio (dB)	< 1
Ports Isolation (dB)	20

III. ORTHOMODE TRANSDUCER DESIGN

Previous orthomode transducer (OMT) designs have provided satisfactory performance in specific applications but generally fall short of addressing the evolving requirements of modern communication systems. Many conventional designs are inherently bulky due to long and intricate waveguide paths with multiple bends, which not only enlarge the device footprint but also complicate integration with other subsystems [33], [34]. The use of non-aligned output ports further limits compatibility with compact and tightly packed architectures such as MIMO satellite arrays, where spatial efficiency is critical.

Another challenge is phase imbalance, which is particularly problematic in circularly polarized systems, where unequal path lengths between orthogonal modes can degrade polarization purity and overall link quality [35]. Many existing designs struggle to maintain precise phase balance across output channels, resulting in reduced reliability and performance consistency. Collectively, these issues highlight the limitations of conventional OMTs and emphasize the need for innovative approaches that deliver compact form factors, integration-friendly geometries, robust system-level resilience, and accurate phase equalization [36], [37].

These challenges have been partially addressed by recent designs [38], but one limitation remains: the overall length of the OMT is still too long. The increased length primarily results from using tall, multi-step twists. These twists help align the ports in a specific manner while maintaining equal electrical path lengths. To reduce this issue, the twist section is decreased to only a three-step configuration instead of six. This change would create a more compact profile without losing electrical balance. In the next section, we will introduce a more compact OMT design that shortens the overall structure and features a new mechanical setup. This new setup aims to simplify fabrication and reduce the number of required fabricated sections.

A. ELECTRICAL DESIGN

The two-fold OMT is composed of two key parts, the central section and the combining network. Both the main section and the combining components have been specially designed and optimized for operation within the Ka-band, spanning a frequency range of 19.5 GHz to 29.5 GHz. The two combining arms are shown in Figure 2 (a); these arms are length optimized, where the separation distance is set to be $l_{center} = 30$ mm with overall length $l_{arm} = 33$ mm. The twists used at the end of each arm are composed of only three steps to decrease the overall length. The center section is composed of three stepped cylinders with reduced radii. Moreover, the width of the overall center section is chosen to be around $W_{center} = 23$ mm, and the common port is

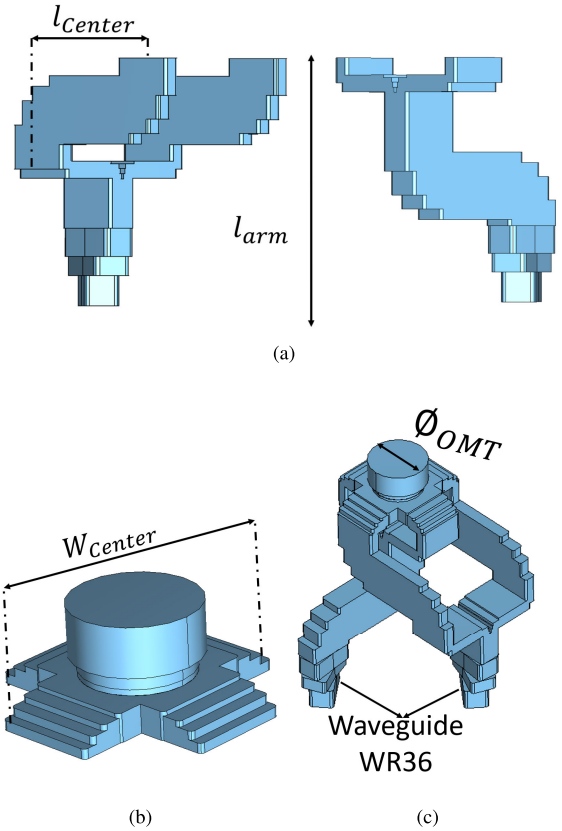

FIGURE 2. Compact OMT design for the satellite feeding structure, (a) combining arms, (b) center section, (c) overall structure (center section + combining arms), and (d) proposed cuts for fabrication.

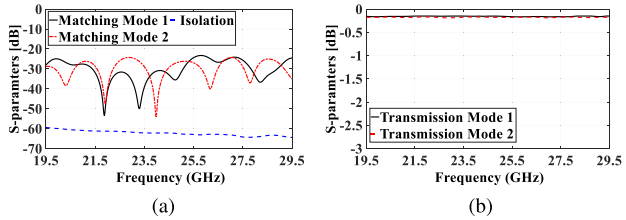

FIGURE 3. Simulation results for OMT using CST microwave studio, (a) matching level with isolation, and (b) transmissions for both modes.

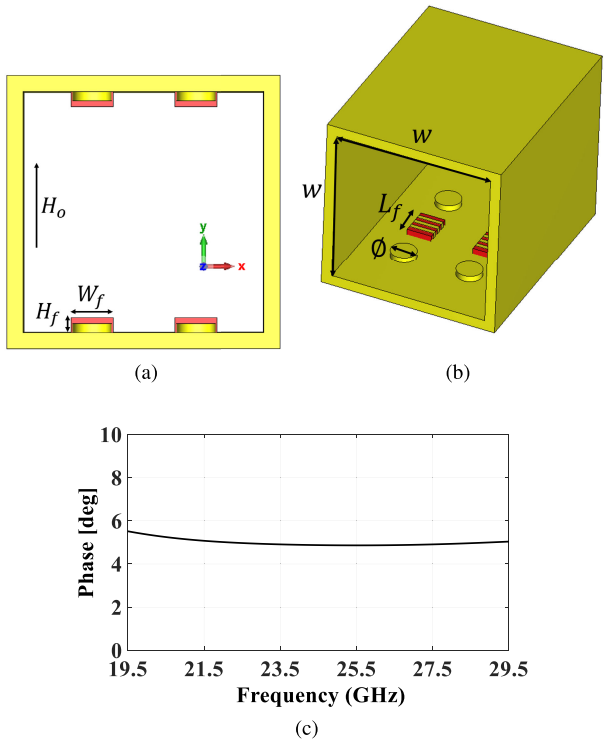

FIGURE 4. Ferrite polarizer configuration, (a) front view, (b) 3D structure, and (c) phase for small section.

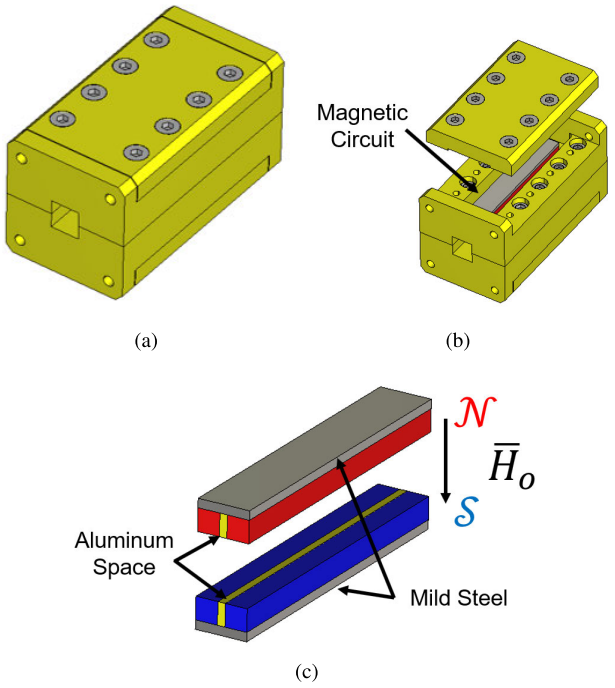

FIGURE 5. Biasing magnetic circuit configuration, (a) polarizer model, (b) circuit overview, and (c) detailed circuit configuration.

ϕ_{OMT} = 5.7 mm. The overall structure is shown in Figure 2, where the rectangular waveguide ports are (0.36×0.18 inch^2) with a cutoff frequency of 16.4 GHz. Additionally, the complete assembly of the structure utilizes

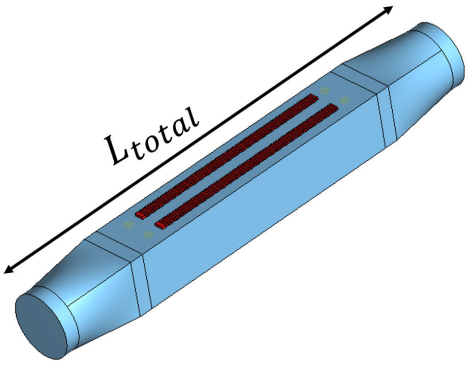

(a)

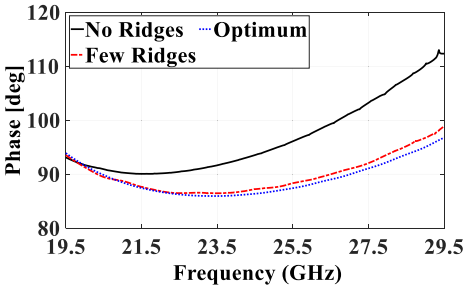

(b)

FIGURE 6. The overall structure for the ferrite phase shifter, (a) 3D model, and (b) output phase response with the effect of the corrugation.

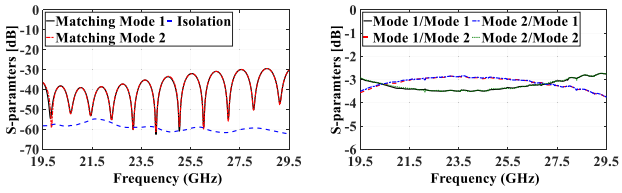

(a) (b)

FIGURE 7. S-parameters simulation results for ferrite polarizer, (a) matching level with isolation, and (b) transmissions for both modes.

innovative cutting planes, which are detailed in the mechanical design section. The overall response for this OMT is shown in Figure 3, where the overall matching level is around 25 dB for both modes, and with a deep isolation level. Moreover, the primary advantage of this design is the insertion loss, which is approximately 0.15 dB due to the reduction in the overall length of the design.

B. MECHANICAL MODEL

The overall assembly model of the OMT consists of seven main parts, carefully designed to ensure proper electrical performance and facilitate the fabrication process. The placed cuts are taken in one direction, as shown in Figure 2. These

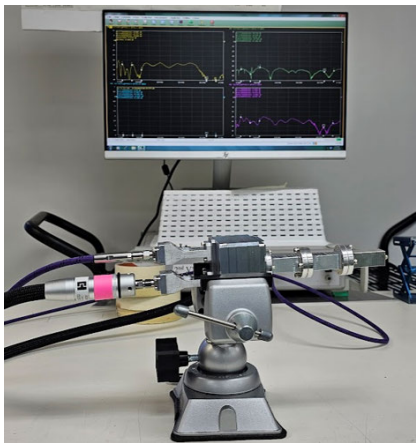

(a)

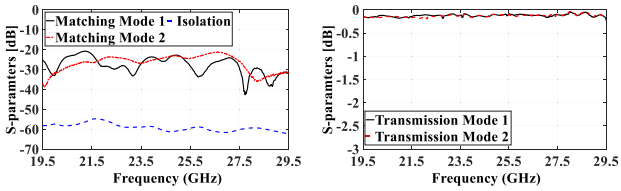

(b) (c)

FIGURE 8. The OMT prototype measurements, (a) fabricated unit, (b) measured matching level and isolation, and (c) measured transmissions for both modes.

cut sections play a crucial role in the overall functionality and construction of the OMT, ensuring efficient operation and streamlined fabrication. The overall weight of the proposed design, using aluminum material, is 0.3 kg. The overall dimensions L_{OMT}, W_{OMT}, H_{OMT} for the proposed design are 50 mm, 50 mm, and 43 mm, respectively.

IV. FERRITE POLARIZER DESIGN

Differential ferrite phase shifters can be realized in several configurations depending on the placement and cross-sectional geometry of the ferrite material, such as rectangular, circular, or square tiles. Among these, rectangular ferrite slabs are most commonly used due to their manufacturability and ease of integration. These slabs can be oriented either vertically or horizontally inside the waveguide, leading to two widely adopted configurations: vertical-tile and horizontal-tile phase shifters [23].

To maximize the achievable differential phase for a given filling factor ($\Delta S/S$), defined as the ratio of the ferrite slab area to the waveguide cross-sectional area, the ferrite must be placed at the circular polarization point inside the rectangular waveguide [23]. At this location, the transverse magnetic field components satisfy the condition of equal magnitude with a 90° phase difference, such that $H_x/H_z = \pm j$.

The optimum position of this circular polarization point is determined by:

$$\tan(k_c x) = \pm \frac{k_c}{\beta_0} \tag{1}$$

TABLE 2. Ferrite material specifications and dimensions.

$4\pi M_s$ (Gauss)	4000
H_o (Oe)	1500
ϵ_r	16
H_f	0.81
W_f	1.65

where $k_c = \pi/a$ is the cutoff wave number and $\beta_0 = \sqrt{k_0^2 - k_c^2}$ is the propagation constant of the air-filled rectangular frequency-dependent, which limits the usable bandwidth. As a result, vertical ferrite slabs generally satisfy this condition over a relatively narrow bandwidth. In contrast, horizontal ferrite slabs can support a wider frequency range while maintaining similar performance [25], [39].

Upon this idea, an innovative extension uses horizontal ferrite slabs inside a square waveguide to create a ferrite-based polarizer. In this setup, four ferrite slabs are used, with two mounted on each side of the square cross-section, mirroring their counterparts on the opposite sides. This layout introduces a controlled phase shift between the two orthogonal propagating modes, resulting in a circularly polarized signal. This polarizer benefits from the natural thermal stability and broad frequency range of horizontal ferrite loading, while also utilizing the nonreciprocal properties of ferrite materials to achieve efficient 90° phase shifting across a practical operating range.

The proposed configuration of the ferrite-based polarizer is shown in Figure 4. The design uses a square waveguide with a side dimension of $W = 10.3632$, mm. To improve impedance matching and reduce reflections, four metallic posts are placed in front of each ferrite slab. This creates a matching section that significantly enhances the return loss characteristics of the device. The phase shift that can be achieved depends on several control parameters. These include the geometric dimensions of the ferrite slabs, the magnetic and dielectric properties of the ferrite material, and the layout of the external magnetic biasing circuit. Together, these factors determine the device's bandwidth, phase accuracy, and overall performance.

A. MAGNETIC BIASING CIRCUIT AND FIELD UNIFORMITY

The mechanical modeling for this polarizer is shown in Figure 5 (a). This model has a cover for protecting the magnetic biasing circuit made from aluminum, as indicated in Figure 5 (b). The magnetic biasing is built as shown in Figure 5. This circuit is composed of four magnetic slabs, two at the top and two at the bottom. Between each of them, there is an aluminum spacer to allocate the magnets above the ferrite slabs directly. Moreover, a mild steel sheet is used to connect these magnets. The mild steel has high magnetic permeability, so it is used to improve the magnetic field and offer a good balance field across the slabs.

B. PHASE SHIFT ANALYSIS

To determine the required ferrite dimensions, a small section of the ferrite polarizer was simulated in order to evaluate the corresponding phase response. The ferrite material was selected with the properties listed in Table 2. Using an initial guess length of $L_f = 2$, mm, the resulting phase shift was approximately 6°, as illustrated in Figure 4. Accordingly, to achieve the target 90° phase shift, the ferrite length can be estimated using the following relation,

$$l_{fnew} = \frac{\theta_{new} \times l_f}{\theta_{old}} \tag{2}$$

The required length of the ferrite slab is 30 mm. However, to achieve a more uniform phase response across the operating band, the slab is segmented into smaller sections and corrugated along the waveguide. These corrugations serve to tailor the propagation characteristics, effectively flattening the phase response, as illustrated in Figure 6. The concept behind using these segmentations or corrugations originates from traditional waveguide polarizer techniques, where such features introduce a phase shift to one of the propagating modes. Additionally, prior work in the literature demonstrates the use of ferrite-slab phase shifters in waveguides. Based on this, our initial approach was to incorporate a ferrite slab directly into a square waveguide; however, the resulting phase response proved unstable. By combining both methods—ferrite loading and corrugation—and carefully fine-tuning their respective parameters.

The polarizer is connected to a transition from a square waveguide to a circular one, to be integrated with the OMT, as shown in Figure 6 with overall length $L_{total} = 85$ mm. The simulated performance of the proposed polarizer is shown in Figure 7. The results reveal a matching level of about 30 dB throughout the entire operating band, with isolation above 50 dB. To account for practical losses, the simulation considers the conductive losses of aluminum and the inherent ferrite losses, modeled with a resonance line width of approximately 16 Oe. The related transmission characteristics under these conditions appear in Figure 7(b).

V. CORRUGATED HORN ANTENNA

A corrugated horn antenna is proposed to evaluate the overall performance and radiation patterns for the OMT with a polarizer. The proposed antenna design requires a good matching level over the whole band of operation, 19.5-29.5 GHz. The input diameter ϕ_{in} of the antenna is chosen to be $\phi_{in} = 0.45$inch followed by a circular waveguide transition as shown in Figure 9 (a). This diameter ensures the propagation of the dominant TE11 mode while avoiding the excitation of higher-order modes. The second section in the horn design is the mode conversion section. A variable-depth slot mode converter is used, typically comprising five slots. The choice of the corrugation profile is another vital consideration that affects the radiation pattern characteristics of the antenna. The hyperbolic profile is

TABLE 3. Comparison between the proposed OMT and the other two-folded designs.

Ref.	Frequency (GHz)	BW%	RL [dB]	Loss [dB/mm]	Isolation [dB]	Size (λ_o^3)
[38]	17.7-31	54.6	25	0.005	50	$4 \times 2.2 \times 6.55$
[13]	67-116	53	20	0.25	60	$18 \times 19 \times 7.6$
[36]	29-50	53	20	0.075	60	$12.11 \times 11.58 \times 4.5$
[37]	18-26	36.36	19	0.004	48	$10.78 \times 10.78 \times 7.04$
[40]	24-42	54.54	20	-	60	-
This work	19.5-29.5	40.5	20	0.004	55	$4 \times 4 \times 3.6$

TABLE 4. Circular polarized systems.

Ref.	Design Type	Center Freq. (GHz)	BW%	RL [dB]	IL [dB]	ISOL [dB]	AR [dB]
[31]	Septum OMT	22	36.36	15	1.7	17	1.3
[32]	Septum OMT	60	16.7	14	1.3	20	1.3
[41]	Microstrip Feeding Network	20 / 30	24.3/10	7/11	-	-	2/2.5
[42]	Quasi-planar Coaxial Waveguide	16 / 33.5	19.4/7.4	10	-	10/15	2
[29]	Couplers + OMT	18.95 / 28.75	13.8/8.4	20	-	17	0.57
[28]	OMT + Polarizer	44.2	37	19.5	-	30	0.35
This Work	OMT + Polarizer	24.5	40	19.8	0.45	30	0.95

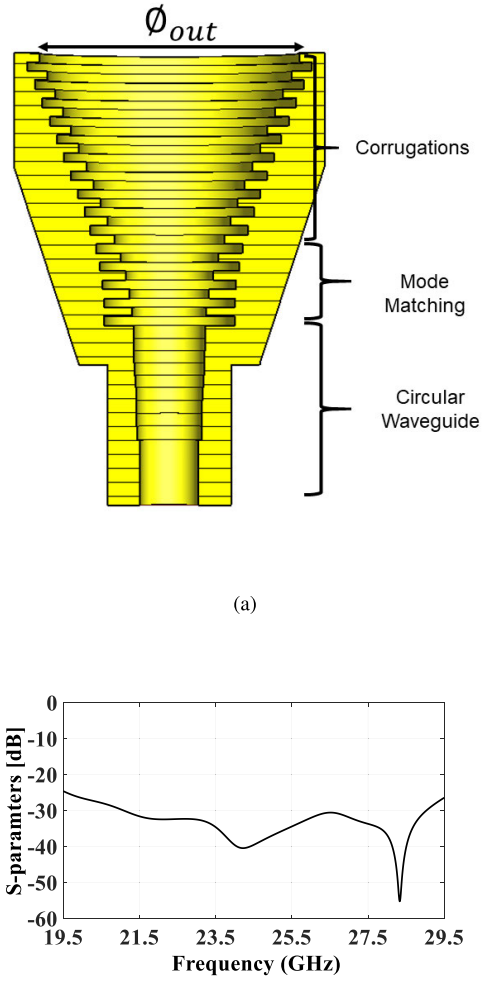

FIGURE 9. The proposed antenna, (a) 3D structure, (b) matching level.

frequently utilized, where the main body of the antenna is constructed using a hyperbolic profile with a variable number of slots. This overall design is modeled using CST Microwave Studio Macros to ease the optimization of changing the number of corrugations in mode conversion and horn body simultaneously. The overall response for the matching level is shown in Figure 9 (b), and the radiation patterns will be discussed in the overall assembly section.

VI. PROTOTYPE FABRICATION AND MEASUREMENTS

Fabrication is executed with a computer numerical control milling machine, ensuring an accuracy of ±0.5 mil. The measurements are carried out using an ANRITSU MS46322A VNA, with waveguide triple offset short calibration. A matched circular load evaluates the matching level for both ports as shown in Figure 8. The matching level for both modes is around 20 dB as shown in Figure 8 (b), with an isolation of 55 dB. The transmission is evaluated by back-to-back measurements with another OMT, and the obtained results are shown in Figure 8 (c), which is around 0.25 dB for both modes.

The proposed OMT is compared to previously published twofold OMT designs, with a summary in Table 3. The table includes key performance metrics, such as return loss (RL), insertion loss (IL), and overall physical dimensions in free-space wavelength at the center frequency (λ_o). A significant issue with most reported designs is their large cross-sectional footprint, which makes them hard to fit into compact platforms such as MIMO satellite systems [13], [36], [37], [40]. Many designs also have excessive overall length because they include double twists and long straight waveguide sections [38]. The proposed OMT solves these problems by providing a more compact shape with lower insertion loss, as shown in Table 3.

VII. OVERALL SATELLITE FEEDING SYSTEM

The measured results from the OMT, are used to evaluate the proposed ferrite polarizer with the antenna. The results are imported into the CST-Microwave Studio by adding the S4P file for the OMT results. The results are taken from the VNA

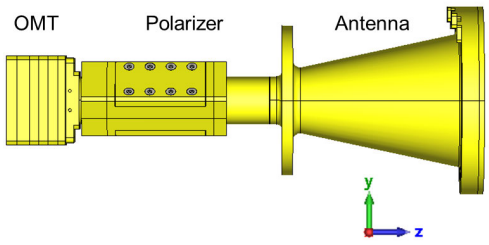

(a)

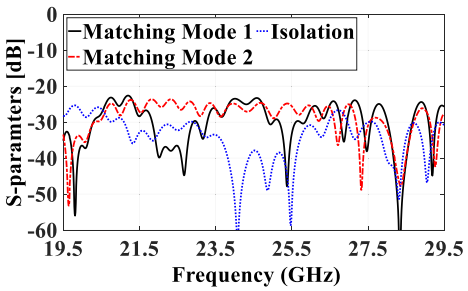

(b)

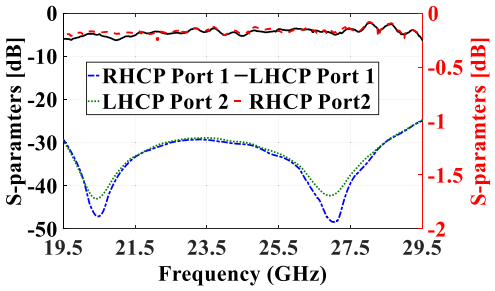

(c)

FIGURE 10. The overall system response, (a) 3D structure, (b) overall matching level and isolation, and (c) overall transmissions with RHCP/LHCP isolations.

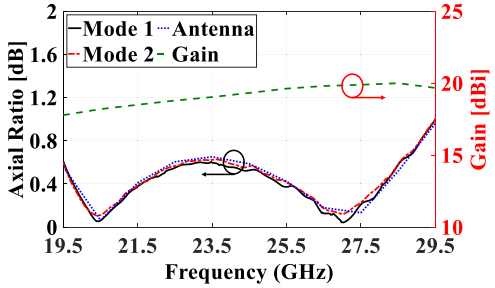

FIGURE 11. The overall response for the axial ratio and gain for both ports of the system.

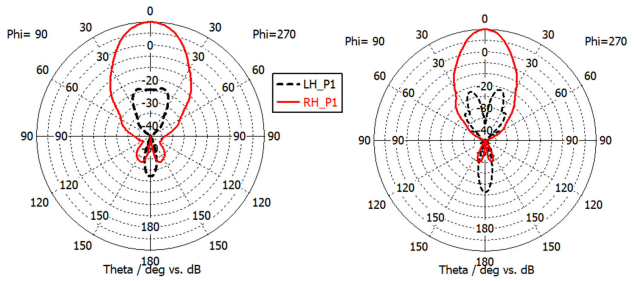

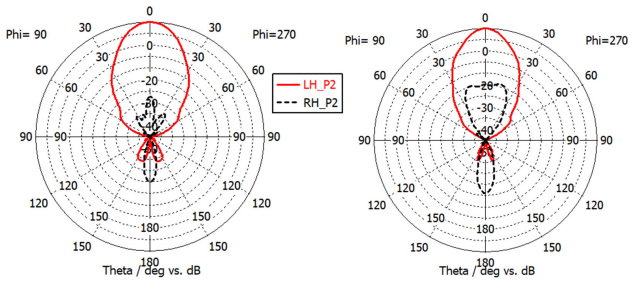

FIGURE 12. The overall radiation patterns, (a) Port 1 at 19.5 GHz, (b) Port 1 at 29.5 GHz, (c) Port 2 at 19.5 GHz, (d) Port 2 at 29.5 GHz.

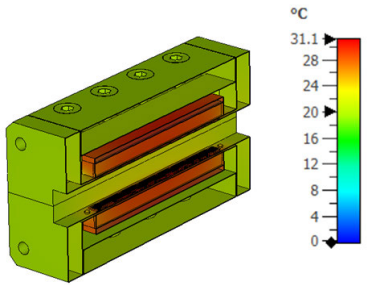

(a)

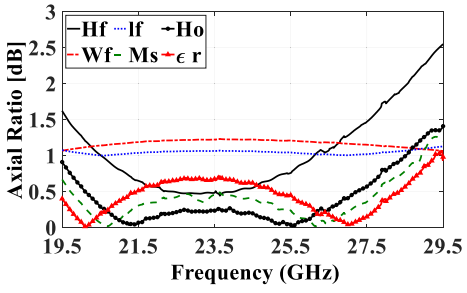

(b)

FIGURE 13. Thermal and tolerance analysis effects, (a) thermal response on the polarizer, and (b) effects on axial ratio.

as S2P files by doing a waveguide calibration. Then these S2P files are used to build the S4P matrix, which is added to the CST, and the overall system shown in Figure 10 (a) is evaluated in terms of S-parameters and the RHCP/LHCP isolation. Afterwards, the OMT and Polarizer are evaluated by adding the corrugated horn antenna to the simulation environment to discuss the radiation patterns. The matching level for the whole system is around 25 dB with an isolation of 28 dB. Moreover, the response for the OMT with the polarizer is showing an insertion loss is around 0.45 dB, with an RHCP/LHCP isolation of approximately 25 dB, as clearly

indicated in Figure 10 (d). Thus, by calculating the axial ratio using the following relation,

$$AR|_{dB} = 20\log\left(\frac{1+10^{\frac{XP}{20}}}{1-10^{\frac{XP}{20}}}\right) \quad (3)$$

The corresponding axial ratio value is around 0.95 dB as indicated in Figure 11 which is comparable to the axial ratio from the antenna. The radiation pattern for the system is indicated in Figure 12, where the first port is responsible for right-hand transmission. The radiation pattern is showing a good LHCP/RHCP isolation for both ports at different frequency points. Moreover, the gain of the system is at the level of 17 dBi, increasing gradually to 20 dBi at the end of the band.

A. THERMAL AND TOLERANCE ANALYSIS

In this section, we are performing a thermal and tolerance analysis for the ferrite section. This analysis gives an intuition of the effect of the parameters on the circular polarization clarity. The thermal analysis is performed using CST Microwave Studio after defining the ferrite material thermal properties, and defining the ambient temperature to be 20°C. Moreover, the peak power is chosen to be around 10 kW, with an average power of 500 W. The resultant analysis shows a small deviation in the temperature of about 10°C as indicated in Figure 13(a). This increase in temperature affects the ferrite dimensions to be 0.001 inch. Thus, a tolerance analysis by 0.001 inch for all ferrite dimensions is applied. Moreover, the magnetization properties M_s & H_o with the electric permittivity are discussed as well. The effects of these parameters on the axial ratio are shown in Figure 13(b). As indicated in the curves, the worst case scenario is shown from the height of the ferrite H_f, however, the other parameters are affecting the axial ratio but within an acceptable range.

B. SYSTEM EVALUATION SECTION AND FUTURE WORKS

Different configurations are summarized in Figure 1. Septum OMT-based systems usually struggle with poor axial ratio performance and have limited bandwidth. Most designs are restricted to about 16% fractional bandwidth [32]. While some methods extend the bandwidth beyond 35%, they often use triangular common ports. These ports are hard to integrate with conventional conical or pyramidal horn antennas [31]. Moreover, some recent designs are proposing a waveguide phase array with a microstrip feeding network [41]. This design bandwidth ratio is good for both operating bands. However, the design response in terms of axial ratio is very high, which is around 2 dB to 2.5 dB. Another design is using a coaxial line [42] to propose a CP system. This design is a dual-band system that achieves a good bandwidth ratio, but lacks in getting a deep matching level, and the axial ratio presented in the paper is in the range of 2 dB.

The second category of CP systems relies on directional couplers and faces a different problem: bandwidth. In these designs, the port isolation is typically around 17 dB. However, they can still achieve a good axial ratio across the operating band [29].

A third approach uses polarizer-based CP systems [28]. In this setup, corrugated irises are added to a circular waveguide. When paired with an OMT, this configuration achieves an overall matching level of approximately 19.5 dB and a near-ideal axial ratio; however, its bandwidth remains limited to around 37%.

This paper introduces a new method for evaluating components in satellite feeding structures. It emphasizes the importance of AI-assisted analysis in today's RF design. This helps designers create circularly polarized systems that meet specific performance needs. Machine learning techniques, such as decision trees, have shown promising outcomes in the parametric modeling of microwave components [43], [44], [45], [46], [47]. Furthermore, AI techniques allow for a clearer position of this work within the current landscape of optimization-focused and antenna feed designs. A broader quantitative comparison with recent AI or optimization-enhanced CP systems used in LEO satellite applications would strengthen the novelty of this approach [48], [49].

VIII. CONCLUSION

This paper presents the design and evaluation of a novel CP system that integrates a compact OMT with a ferrite polarizer and a courrgated horn antenna for satellite communication applications. The OMT we propose offers low insertion loss, high return loss, and smaller dimensions, solving key problems found in traditional twofold OMTs, which are often too long and hard to integrate in MIMO satellite systems. A comparison with septum OMTs, coupler-based CP systems, and polarizer-based methods shows the benefits of our design. The ferrite polarizer uses segmented slabs with matching posts, ensuring a flat phase response and thermal stability. This gives reliable performance in space. The OMT is fabricated and measured, showing good agreement with the simulated response. The OMT measurements are used in CST to evaluate the proposed polarizer with the antenna. In the band of 19.5-29.5 GHz, the overall system achieves a good balance between bandwidth, axial ratio, isolation, and ease of integration.

ACKNOWLEDGMENT

The authors would like to express their sincere gratitude to Prof. Abdelrazik Sebak's research group for their technical support, constructive discussions, and continuous encouragement, which greatly contributed to this research. They would like to thank Scientific Microwave Corporation (SMC), Montreal, QC, Canada for their technical assistance in fabricating the experimental prototype.

REFERENCES

[1] P. Sohrabi, P. Rezaei, S. Kiani, and M. Fakhr, "A symmetrical SIW-based leaky-wave antenna with continuous beam scanning from backward-to-forward through broadside," *Wireless Netw.*, vol. 27, no. 8, pp. 5417–5424, Nov. 2021.

[2] H. R. Heidari, P. Rezaei, S. Kiani, and M. Taherinezhad, "A monopulse array antenna based on SIW with circular polarization for using in tracking systems," *AEU - Int. J. Electron. Commun.*, vol. 162, Apr. 2023, Art. no. 154563.

[3] S. Kiani, P. Rezaei, and M. Fakhr, "A CPW-fed wearable antenna at ISM band for biomedical and WBAN applications," *Wireless Netw.*, vol. 27, no. 1, pp. 735–745, Jan. 2021.

[4] Y. Du, S. Liu, Z. Fang, and S. Gao, "Reliability evaluation of all-user terminals in LEO satellite communication network based on modular reduction," *China Commun.*, vol. 19, no. 2, pp. 235–246, Feb. 2022.

[5] L. Jin, L. Wang, X. Jin, J. Zhu, K. Duan, and Z. Li, "Research on the application of LEO satellite in IoT," in *Proc. IEEE 2nd Int. Conf. Electron. Technol., Commun. Inf. (ICETCI)*, May 2022, pp. 739–741.

[6] C. S. Kim, "Ku-band circular/linear polarized feed system design," in *IEEE Antennas Propag. Soc. Int. Symp. Dig.*, vol. 2, Aug. 2002, pp. 918–921.

[7] M. Gadelrab, S. I. Shams, and A. R. Sebak, "Dual linear polarized antenna feed for LEO satellites," in *Proc. Int. Telecommun. Conf. (ITC-Egypt)*, Egypt, Jul. 2022, pp. 1–4.

[8] B. G. Evans, *Satellite Communication Systems*, vol. 38. Stevenage, U.K.: IET, 1999.

[9] F. A. Dicandia, S. Genovesi, and A. Monorchio, "Analysis of the performance enhancement of MIMO systems employing circular polarization," *IEEE Trans. Antennas Propag.*, vol. 65, no. 9, pp. 4824–4835, Sep. 2017.

[10] H.-T. Hsu, Y.-F. Tsao, and A. Desai, "Dual-wideband antenna with dual polarization and enhanced front-to-back ratio for high-speed communication applications," *AEU-Int. J. Electron. Commun.*, vol. 174, Jan. 2024, Art. no. 155072.

[11] A. Bagheri, M. Khodadadi, T. Brown, P. Xiao, and M. Khalily, "Single-feed, dual-polarized transmissive metasurface antenna for 5G applications," *AEU-Int. J. Electron. Commun.*, vol. 191, Feb. 2025, Art. no. 155652.

[12] A. M. Bøifot, "Classification of ortho-mode transducers," *Eur. Trans. Telecommun.*, vol. 2, no. 5, pp. 503–510, 1991.

[13] I. Barrueto, N. Reyes, P. Mena, and L. Bronfman, "A broadband orthomode transducer for the new ALMA band 2+3 (67–116 GHz)," in *Proc. Global Symp. Millim. Waves (GSMM) ESA Workshop Millimetre-Wave Technol. Appl.*, Jun. 2016, pp. 1–4.

[14] S.-G. Park, H. Lee, and Y.-H. Kim, "A turnstile junction waveguide orthomode transducer for the simultaneous dual polarization radar," in *Proc. Asia–Pacific Microw. Conf.*, Dec. 2009, pp. 135–138.

[15] J. A. Ruiz-Cruz, J. R. Montejo-Garai, and J. M. Rebollar, "Optimal configurations for integrated antenna feeders with linear dual-polarisation and multiple frequency bands," *IET Microw., Antennas Propag.*, vol. 5, no. 8, pp. 1016–1022, Jun. 2011.

[16] M. Gadelrab, S. I. Shams, and A. Sebak, "Compact dual linear polarized antenna feed for LEO satellites based on quad ridge waveguide," in *Proc. Int. Telecommun. Conf. (ITC-Egypt)*, Jul. 2023, pp. 210–214.

[17] J. Zhang, B. Zhang, H. Deng, B. Dai, X. Chen, Z. Niu, Y. Feng, and Y. Fan, "170–260-GHz ultrawideband and high isolation orthomode transducer based on symmetric reverse coupling structure," *IEEE Trans. Microw. Theory Techn.*, vol. 71, no. 5, pp. 2169–2177, May 2023.

[18] S. Piltyay, A. Bulashenko, O. Sushko, O. Bulashenko, and I. Demchenko, "Analytical modeling and optimization of new Ku-band tunable square waveguide iris-post polarizer," *Int. J. Numer. Model., Electron. Netw., Devices Fields*, vol. 34, no. 5, p. 2890, Aug. 2021.

[19] G. Bertin, B. Piovano, L. Accatino, and M. Mongiardo, "Full-wave design and optimization of circular waveguide polarizers with elliptical irises," *IEEE Trans. Microw. Theory Techn.*, vol. 50, no. 4, pp. 1077–1083, Apr. 2002.

[20] S. I. Piltyay, "High performance extended C-band 3.4–4.8 GHz dual circular polarization feed system," in *Proc. 11th Int. Conf. Antenna Theory Techn. (ICATT)*, May 2017, pp. 284–287.

[21] M.-H. Chung, D.-H. Je, S.-T. Han, and S.-R. Kim, "Development of a 85–115 GHz 90-deg phase shifter using corrugated square waveguide," in *Proc. 44th Eur. Microw. Conf.*, Oct. 2014, pp. 1146–1149.

[22] A. Polishchuk, A. Bulashenko, S. Piltyay, O. Bulashenko, and I. Zabegalov, "Compact posts-based waveguide polarizer for satellite communications and radar systems," in *Proc. IEEE 3rd Ukraine Conf. Electr. Comput. Eng. (UKRCON)*, Aug. 2021, pp. 78–83.

[23] D. M. Pozar, *Microwave Engineering*, 4th ed., Hoboken, NJ, USA: Wiley, 2009.

[24] J. R. Bray and L. Roy, "Development of a millimeter-wave ferrite-filled antisymmetrically biased rectangular waveguide phase shifter embedded in low-temperature cofired ceramic," *IEEE Trans. Microw. Theory Techn.*, vol. 52, no. 7, pp. 1732–1739, Jul. 2004.

[25] M. G. Ahmed, M. M. M. Ali, S. I. Shams, M. Elsaadany, and A. M. M. A. Allam, "Ferrite isolator based on dual non-reciprocal mode converting in rectangular waveguide," in *Proc. 15th Eur. Conf. Antennas Propag. (EuCAP)*, Mar. 2021, pp. 1–4.

[26] C. Şahin and S. Şimsek, "Analysis and design of differential phase shifter based on ferrite loaded rectangular waveguide," in *Proc. 11th Int. Conf. Electr. Electron. Eng. (ICEEE)*, Apr. 2024, pp. 16–20.

[27] M. Gadelrab, "LEO satellite feeding system: Design and analysis," Ph.D. dissertation, Dept. Elect. Comput. Eng., Concordia University, Montreal, QC, Canada, 2023.

[28] R. Roberts, P. Booth, G. Fox, S. Stirland, and M. Simeoni, "Q/V-band feed system development," in *Proc. 10th Eur. Conf. Antennas Propag. (EuCAP)*, Apr. 2016, pp. 1–5.

[29] M. Gadelrab, S. I. Shams, M. Elsaadany, and G. Gagnon, "Design of corrugated horn antenna for LEO satellite feeding system: Efficient hybrid optimization approach," *IEEE Access*, vol. 13, pp. 92730–92739, 2025.

[30] P. Kohl, M. Kilian, M. Schneider, and C. Hartwanger, "A compact dual band polariser for Q/V-band," in *Proc. 14th German Microw. Conf. (GeMiC)*, May 2022, pp. 9–12.

[31] B. Deutschmann and A. F. Jacob, "Broadband septum polarizer with triangular common port," *IEEE Trans. Microw. Theory Techn.*, vol. 68, no. 2, pp. 693–700, Feb. 2020.

[32] S. Shams, A. M. Mahfouz, M. Elsaadany, M. A. M. Hassan, G. Gagnon, and A. A. Kishk, "Circularly polarized V-band orthomode transducer," *IEEE Antennas Wireless Propag. Lett.*, vol. 22, no. 1, pp. 29–33, Jan. 2023.

[33] S. Srikanth and M. Solatka, "A compact full waveguide band turnstile junction orthomode transducer," in *Proc. 30th URSI Gen. Assem. Scientific Symp.*, Aug. 2011, pp. 1–4.

[34] D. Dousset, S. Claude, and K. Wu, "A compact high-performance orthomode transducer for the Atacama large millimeter array (ALMA) band 1 (31–45 GHz)," *IEEE Access*, vol. 1, pp. 480–487, 2013.

[35] D. Henke, N. Kelly, K. Marshall, I. Wevers, and L. B. G. Knee, "A turnstile quad-ridge orthomode transducer (OMT) for octave-bandwidth receiver front-ends (24–51 GHz)," *IEEE Trans. Microw. Theory Techn.*, vol. 71, no. 11, pp. 4906–4921, Nov. 2023.

[36] C.-C. Chiong, C. Chien, C.-C. Chang, Y. De Huang, and Y.-J. Hwang, "Cryogenic 29–50 GHz orthomode transducer for radio astronomical receiver," in *Proc. Asia–Pacific Microw. Conf. (APMC)*, Nov. 2018, pp. 1271–1273.

[37] A. Navarrini and R. L. Plambeck, "A turnstile junction waveguide orthomode transducer," *IEEE Trans. Microw. Theory Techn.*, vol. 54, no. 1, pp. 272–277, Jan. 2006.

[38] M. Gadelrab, S. I. Shams, M. Elsaadany, and A. Sebak, "Compact wideband twofold orthomode transducer," *AEU–Int. J. Electron. Commun.*, vol. 200, Oct. 2025, Art. no. 155929.

[39] M. A. Abdelaal, S. I. Shams, and A. A. Kishk, "Rectangular waveguide differential phase shifter based on horizontal ferrite tiles: Accurate model for full-band operation," *IEEE Access*, vol. 7, pp. 23766–23778, 2019.

[40] J. Xiao, G. Teni, H. Li, T. Ding, and Q. Ye, "A dual-polarized horn antenna covering full Ka-band using turnstile OMT," *Frontiers Phys.*, vol. 10, Apr. 2022, Art. no. 880606.

[41] Y. Wei, C. Arnold, and J. Hong, "Multiport beamforming system based on reconfigurable waveguide phased antenna array for satellite communication applications," *IEEE Access*, vol. 11, pp. 29909–29917, 2023.

[42] J. Ran, Y. Wu, C. Jin, P. Zhang, and W. Wang, "Dual-band multipolarized aperture-shared antenna array for Ku-/Ka-band satellite communication," *IEEE Trans. Antennas Propag.*, vol. 71, no. 5, pp. 3882–3893, May 2023.

[43] F. Feng, W. Na, J. Jin, J. Zhang, W. Zhang, and Q.-J. Zhang, "Artificial neural networks for microwave computer-aided design: The state of the art," *IEEE Trans. Microw. Theory Techn.*, vol. 70, no. 11, pp. 4597–4619, Nov. 2022.

[44] F. Feng, X. Wang, W. Liu, J. Xue, W. Liu, J. Zhang, W. Zhang, and Q.-J. Zhang, "A novel EM parametric modeling method of microwave filters incorporating multivalued neural networks and transfer functions," *IEEE Trans. Microw. Theory Techn.*, vol. 72, no. 11, pp. 6360–6374, Nov. 2024.

[45] J. Cui, R. Chen, F. Feng, J. Wang, J. Zhang, W. Liu, K. Ma, and Q.-J. Zhang, "Advanced Bayesian-inspired multilayer effective parameter determination method for automated ANN model generation of microwave components," *IEEE Trans. Microw. Theory Techn.*, vol. 72, no. 8, pp. 4408–4420, Aug. 2024.
[46] A. Ibrahim, S. Mohamed, M. Gadelrab, M. Elsaadany, and S. I. Shams, "Wideband corrugated horn design based on machine learning technique," in *Proc. IEEE 20th Int. Symp. Antenna Technol. Appl. Electromagn.*, Jul. 2025, pp. 32–35.
[47] N. Issa, S. Mohamed, M. Gadelrab, M. Elsaadany, and S. I. Shams, "Crossguide coupler design using deep-learning model," in *Proc. IEEE 20th Int. Symp. Antenna Technol. Appl. Electromagn.*, Jul. 2025, pp. 24–27.
[48] N. S. Jonnala, S. Siraaj, Y. Prastuti, P. Chinnababu, B. P. Babu, S. Bansal, P. Upadhyaya, K. Prakash, M. R. I. Faruque, and K. S. Al-Mugren, "AER U-Net: Attention-enhanced multi-scale residual U-Net structure for water body segmentation using Sentinel-2 satellite images," *Sci. Rep.*, vol. 15, no. 1, p. 16099, May 2025.
[49] N. S. Jonnala, R. C. Bheemana, K. Prakash, S. Bansal, A. Jain, V. Pandey, M. R. I. Faruque, and K. S. Al-Mugren, "DSIA U-Net: Deep shallow interaction with attention mechanism UNet for remote sensing satellite images," *Sci. Rep.*, vol. 15, no. 1, p. 549, Jan. 2025.

MAHMOUD GADELRAB (Student Member, IEEE) received the B.Sc. degree in communications engineering from German University in Cairo (GUC), in 2021, and the Master of Applied Science degree from Concordia University in 2023, where he was awarded the Concordia Supervisor's Research Grant. His research interests include ferrite-based structures, ridge gap waveguide technologies, and satellite feeding structures. He received a GUC Top Ranking Students Scholarship, in 2016, and maintained this award, till 2021.

SHOUKRY I. SHAMS (Senior Member, IEEE) received the B.Sc. (Hons.) and M.Sc. degrees in electronics and communications engineering from Cairo University, Cairo, Egypt, in 2004 and 2009, respectively, and the Ph.D. degree in electrical and computer engineering from Concordia University, Montreal, QC, Canada, in 2016. From 2005 to 2006, he was a Teaching and Research Assistant with the Department of Electronics and Communications Engineering, Cairo University. From 2006 to 2012, he was a Teaching and Research Assistant with the Institute of Engineering and Technology (IET) Department, German University in Cairo, Cairo. From 2012 to 2016, he was a Teaching and Research Assistant with Concordia University. His research interests include microwave reciprocal/nonreciprocal design and analysis, high-power microwave subsystems, antenna design, and material measurement. He received the Faculty Certificate of Honor, in 1999, and the Distinction with Honor, in 2004, from Cairo University. He was a recipient of the Concordia University Recruitment Award, in 2012, and the Concordia University Accelerator Award, in 2016. He was German University in Cairo (GUC)-IEEE Student Branch Chair, from 2010 to 2012.

MAHMOUD ELSAADANY (Senior Member, IEEE) received the B.Sc. (Hons.) and M.Sc. degrees in electrical engineering from Cairo University, Giza, Egypt, in 2006 and 2010, respectively, and the Ph.D. degree in electrical and computer engineering from Concordia University, Montreal, QC, Canada, in 2018. He was a Researcher with Qatar University, Doha, Qatar, from 2008 to 2010. He is currently an Assistant Professor with the ECE Department, Concordia University, and a Research Professional with École de Technologie Supérieure (ETS), Université du Québec, Montreal. His current research interests include digital signal processing, optimization of microwave components, machine-type communication, and algorithm design for 5G cellular networks.

GHYSLAIN GAGNON (Senior Member, IEEE) received the Ph.D. degree in electrical engineering from Carleton University, Ottawa, ON, Canada, in 2008. He was the Director of the LACIME Research Laboratory, from 2013 to 2020, a group of 15 professors and 150 highly dedicated students and researchers in microelectronics, digital signal processing, and wireless communications. He is currently a Full Professor and the Dean of Research with the École de technologie supérieure, Université du Québec, Montréal, QC, Canada. His research interests include CMOS IC design, digital signal processing, and machine learning with various applications. He is highly inclined toward collaborative research with industry and was awarded the 2020 Partnership and Innovation Award from ADRIQ.